Chaos, Solitons and Fractals 171 (2023) 113468

Contents lists available at ScienceDirect

Chaos, Solitons and Fractals

journal homepage: www.elsevier.com/locate/chaos

Exact solutions through symmetry reductions for a high-grade brain tumor model with response to hypoxia

M. Rosa [a,b,*], M.L. Gandarias [a], A. Niño-López [a,b], S. Chulián [a,b]

[a] Department of Mathematics, Universidad de Cádiz, Puerto Real, Cádiz, Spain
[b] Biomedical Research and Innovation Institute of Cádiz (INiBICA), Cádiz, Spain

ARTICLE INFO

Keywords:
Lie symmetry
Exact solutions
Brain tumors

ABSTRACT

Mathematical biology models can simulate cell behavior scenarios, specifically for tumor proliferation. In this paper, we study a continuous model describing the evolution of high-grade gliomas from the point of view of the theory of symmetry reductions in partial differential equations (PDEs). Malignant gliomas are the most frequent and deadly type of brain tumor. Over the last few years, complex mathematical models of cancerous growths have been developed increasingly, especially on solid tumors, in which growth primarily comes from abnormal cellular proliferation. The presented PDE system includes two different cellular phenotypes, depending on their oxygenation level. Furthermore, this mathematical model assumes that both phenotypes differ in migration and proliferation rates. Specifically, it includes the possibility of hypoxic cells diffusing into well-oxygenated areas of a tumor. Our main findings are obtained through the classical symmetries admitted by the proposed system, and transformation groups are used to reduce the PDE system to ordinary differential equations. By these means, we provide not only exact solutions but also capture a 3-dimensional representation of the biological phenomenon. The simulations provided show the relationship between normoxic and hypoxic phenotypes in high-grade gliomas.

1. Introduction

High-grade gliomas are tumors of the glial cells found in the brain and spinal cord. They are called "high-grade" because these tumors are fast-growing and spread quickly through brain tissue, making them hard to treat. Median survival is generally less than one year from the moment of diagnosis. Even in the most favorable situations, most patients die within two years [1], with only slight improvement in prognosis in recent years [2]. One of the main reasons for this is the infiltrative character of tumor cells, promoted by the emission of growth factors that are released under hypoxic conditions, i.e., lack of oxygen [3].

Mathematical modeling is a powerful tool for analyzing biological problems. These models can potentially become useful against cancer in three ways: in personalized medicine, accessing unreachable scales, and formulating novel hypotheses [4]. For example, the relationship between proliferation and migration in high-grade gliomas has already been addressed by the mathematical community [5–7] (see [8] for an extended review). Using these methods, several biologically-grounded solutions have been found for different problems in tumor dynamics based on mathematical modeling. For example, in [9], tumor progression and cell motility were studied at the interface between gray and white brain matter, while in [10], some generalizations were included regarding the proliferation rate, being interpreted in terms of the total mass of the tumor.

Here, we consider a reduced continuous model describing the evolution of high-grade gliomas in response to hypoxic events through the interplay of different cellular phenotypes. This model was studied in [11] to show how hypoxic events may have a role in accelerating the growth speed of high-grade gliomas. Previously, the authors considered other models in which they incorporated other phenomena. For example, in [12], a mathematical model was developed which incorporated the interplay among two tumor cell phenotypes, a necrotic core, and the oxygen distribution. This work showed how the collapse of tumor microvessels leads to slower glioma invasion. Also, in [13], a study was proposed based on a mathematical model showing how hypoxic events in space had a crucial part in the acceleration of the growth speed of gliomas under the go or grow hypothesis.

Analytical solutions are rare and difficult to obtain. Hence, searching for exact solutions to nonlinear PDEs plays a fundamental role in analyzing nonlinear physical phenomena. Moreover, very few studies search for exact solutions in cancer models. In [14], an explicit analytical solution was presented for a general two-type birth–death branching

* Corresponding author at: Department of Mathematics, Universidad de Cádiz, Puerto Real, Cádiz, Spain.
E-mail address: maria.rosa@uca.es (M. Rosa).

https://doi.org/10.1016/j.chaos.2023.113468
Received 4 January 2023; Received in revised form 13 April 2023; Accepted 15 April 2023
Available online 4 May 2023

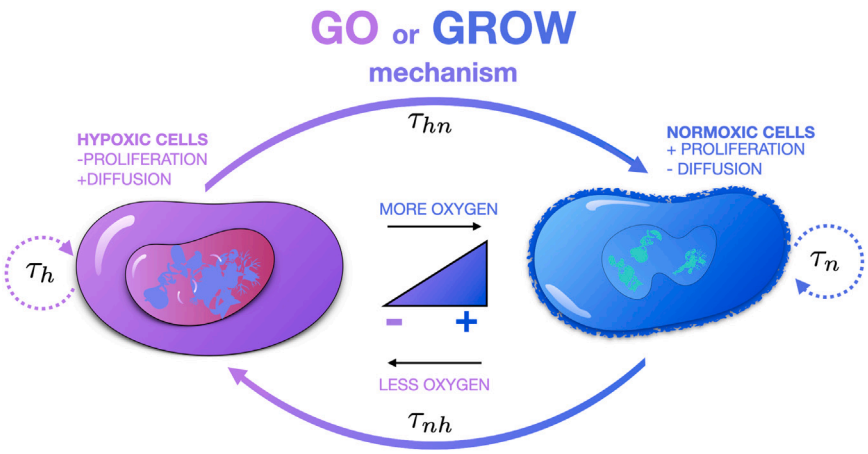

Fig. 1. Oxygenation levels influence tumor cell phenotype. A normal or lower oxygen level determines the normoxic or hypoxic phenotype in cancer cells, respectively. These cells can switch from hypoxic to normoxic (τ_{hn}) and from normoxic to hypoxic (τ_{nh}). A higher level of oxygen drives proliferation, whereas fewer oxygen levels lead to motile cells.

process with one-way mutation. In [15], some exact solutions were derived for a model of growth and movement of certain cell cultures and solid tumors in response to an arbitrary distribution of nutrients. One of the most famous and established procedures for obtaining exact solutions of differential equations is the classical symmetries method, also called group analysis. The investigation of symmetries has manifested as one of the most significant and fundamental methods in almost every branch of science, including mathematics and physics. Among the many papers using this method are [16–18]. Several authors have studied this mathematically-based problem from the oncology field in other contexts. To our knowledge, the application of Lie symmetry analysis is relatively new to the biomathematical literature [19,20]. Lie symmetries are very useful in the theory of nonlinear PDEs and are one of the most efficient tools for constructing exact solutions. As such, they have been successfully employed in recent models [21–25] to obtain applicable solutions in several problems from physical sciences. Traveling fronts of the Lotka–Volterra systems, which have similar structures to the system in study (see system (1) investigated below), have been previously constructed in [26–28]. Moreover, other works such as [29,30] (see also citation therein) have applied Q-conditional symmetries to obtain solutions of Lotka–Volterra type systems.

In [11], the authors presented the results of 1-dimensional numerical simulations showing the acceleration of invasion by waves of cells with a hypoxic phenotype. In this study, we generalize this previous model and, using Lie symmetry groups, find analytical solutions for several models of high-grade brain tumors. This work aims to look for exact solutions using Lie symmetries which describe the previously proposed scenario: the reproduction of how hypoxia in cancer can lead to fast glioma progression. This effect can be shown by how hypoxic cells have a higher diffusive phenotype, whereas normoxic cells are more proliferative than the latter.

The structure of the paper is as follows: In Section 2, a description of the mathematical model consisting of normoxic and hypoxic cells is included; in Section 3, the Lie Symmetries of such system are proposed; finally, in Section 4, these previous results are used to obtain some exact solutions of the model with biological meaning, and then simulate such solution and provide an interpretation.

2. Description of the mathematical model

A cancer model intends to describe certain aspects observed by clinicians and biologists. In the field of oncology, there exist a large number of aspects that, in principle, should be taken into account when designing a model, for example, the different phenotypes of cells, the family of nutrients and oxygen, the vasculature, and other aspects. Malignant gliomas are the most common and lethal type of primary brain tumor. Hypervascularized areas characterize these tumors under moderate levels of hypoxia (deficit in oxygenation) [31]. Hypoxia is a feature encountered in most solid tumors and displays a central role in tumor progression and therapy resistance.

In this work, it is considered the mathematical model described by [11], where it was proposed the idea that the effects of hypoxia may be more perverse than initially considered in previous works [12,13]. Even minimal amounts of hypoxic events may lead to accelerated progression in gliomas. To do this, following the idea behind the go or grow dichotomy described in Fig. 1, the tumor was described as consisting of two subpopulations corresponding to two different tumor phenotypes: a proliferative (or normoxic) one to be denoted as u_n and a migratory (or hypoxic) one u_h. In this model, the force driving phenotype changes is the local oxygen pressure. The term τ_{nh} represents the characteristic time of change of tumor cells to a mobile phenotype in hypoxic conditions. On the contrary, under normoxia, tumor cells acquire a proliferative phenotype in a time τ_{hn} (see, e.g., [12,13]).

Then, in [11], using a reduced model intended to capture the essentials of a striking phenomenon: the acceleration of tumor invasion due to sporadic hypoxic events. Due to this, it was assumed that an initial hypoxic event around a vessel induces a complete phenotype switch of cells around it to a migratory phenotype. Initially, $u_n(x, t = 0)$, $u_h(x, t = 0) = u_h^0(x)$ was taken as tumor density around a tumor vessel. Once the oxygen supply was restored, and considering that oxygenation was maintained above the hypoxia level at all times, the oxygenation level was increased. Due to this biological reasoning, the phenotypic° switch from normoxic to hypoxic cells was omitted (τ_{nh}). In that scenario, a particular case of coupled Fisher–Kolmogorov equations (see [32]),

$$\begin{cases} \dfrac{\partial u_n}{\partial t} = D_n \dfrac{\partial^2 u_n}{\partial x^2} + \dfrac{1}{\tau_n}(1 - u_n - u_h)u_n + \dfrac{1}{\tau_{hn}}u_h, \\ \dfrac{\partial u_h}{\partial t} = D_h \dfrac{\partial^2 u_h}{\partial x^2} + \dfrac{1}{\tau_h}(1 - u_n - u_h)u_h - \dfrac{1}{\tau_{nh}}u_h, \end{cases} \tag{1}$$

described the dynamics, where D_n, D_h are the diffusion coefficients for the normoxic (proliferative) and hypoxic (migratory) phenotypes respectively. The doubling times are τ_n, τ_h for both phenotypes and τ_{hn} is characteristic time for the decay of hypoxic cells into the normoxic phenotype.

In this paper, the model written in (1) was generalized in the following manner: Here $u(t, x, y, z)$ denotes a proliferative (or normoxic) phenotype, and $v(t, x, y, z)$ denotes a migratory (or hypoxic) phenotype, where the force driving phenotype changes is the local oxygen pressure. We considered the independent variables t as the time and x, y, z as the

3-dimensional space. This model is based on a pair of coupled Fisher–Kolmogorov equations (or diffusive Lotka–Volterra equations [33–35]), but including a coupling term accounting for the decay of hypoxic cells into the normoxic phenotype [11]. The generalized model is described by the equations

$$\begin{cases} F_1 \equiv u_t - d_1(u_{xx} + u_{yy} + u_{zz}) - \rho_1(1-u-v)u - g(v) = 0, \\ F_2 \equiv v_t - d_2(v_{xx} + v_{yy} + v_{zz}) - \rho_2(1-u-v)v + g(v) = 0, \end{cases} \tag{2}$$

where d_1 and d_2 are the diffusion coefficients for the proliferative and migratory phenotypes. These parameters satisfy $d_2 > d_1$, and ρ_1, ρ_2 are the proliferation rates for both phenotypes with $\rho_1 > \rho_2$. System (2) is then a generalization of the prior system (1). The function $g(v)$ corresponds to the migratory phenotype switch, changing from the proliferative type to a hypoxic one, where there is a lack of oxygen.

3. Lie symmetries of system (2)

We present the corresponding Lie symmetry analysis for system (2) with arbitrary parameters d_1, d_2, ρ_1, ρ_2 and arbitrary function $g(v)$. This system is a particular case of the generalized systems found [36,37], where the Lie symmetries were derived. However, we explicitly expose these calculations as a means to later exploit exact solutions with biological reasoning. The method for finding Lie point symmetries is well known; see, for example, [19,20,38].

Let us consider a one-parameter Lie group of infinitesimal transformations in (t, x, y, z, u, v). The invariance of system (2) under a Lie group of transformations with an infinitesimal generator of the form

$$X = \tau\frac{\partial}{\partial t} + \xi^1\frac{\partial}{\partial x} + \xi^2\frac{\partial}{\partial y} + \xi^3\frac{\partial}{\partial z} + \eta^1\frac{\partial}{\partial u} + \eta^2\frac{\partial}{\partial v} \tag{3}$$

yields a system of equations for the coordinates $\tau = \tau(t,x,y,z,u,v)$, $\xi^1 = \xi^1(t,x,y,z,u,v)$, $\xi^2 = \xi^2(t,x,y,z,u,v)$, $\xi^3 = \xi^3(t,x,y,z,u,v)$, $\eta^1 = \eta^1(t,x,y,z,u,v)$ and $\eta^2 = \eta^2(t,x,y,z,u,v)$.

Applying the second prolongation $pr^{(2)}X$ to system (2) yields an overdetermined system of linear partial differential equations. The symmetry determining Equation splits with respect to the x-derivatives, y-derivatives, z-derivatives and t-derivatives of u and v, resulting in an overdetermined linear system of equations for the infinitesimals. To compute the determining equations, we used the software Maple (version 2018), and subsequently applied the functions "rifsimp", "dsolve", and "pdsolve" to solve the system. Specifically, "rifsimp" generates a tree with all the solution cases and then, for each solution case, function "dsolve" is applied to find function g(v) and "pdsolve" to find the infinitesimals $\tau(x,y,z,t,u,v)$, $\xi^i(x,y,z,t,u,v), i = 1,2,3$ and $\eta^j(x,y,z,t,u,v), j = 1,2$.

After solving the determining equations, different cases can be distinguished, as shown in Appendix, in which the symmetries are admitted by system (2) for functional forms of $g(v)$. We distinguish as well the corresponding generators and group transformations, depending on three cases. Unfortunately, the conditions $d_1 = d_2$ and $\rho_1 = \rho_2$ need to be fulfilled in Cases 2 and 3, leading to non-biologically grounded transformations. Such cases are given below:

Case 1. For $g = g(v)$ arbitrary function and d_1, d_2, ρ_1, ρ_2 arbitrary constants after solving the determining equations (see determining equations in Appendix A.1), the generators (already given in P.268 from [36]), are:

$$X_1 = \partial_t,\ X_2 = \partial_x,\ X_3 = \partial_y,\ X_4 = \partial_z \tag{4a}$$

(*translations*),

$$X_5 = -y\partial_x + x\partial_y,\ X_6 = -z\partial_x + x\partial_z,\ X_7 = -z\partial_y + y\partial_z \tag{4b}$$

(*rotations*).

These symmetries generate the respective transformation groups:

$$\begin{aligned} &X_1 : t \to t+\epsilon; X_2 : x \to x+\epsilon; X_3 : y \to y+\epsilon; X_4 : z \to z+\epsilon; \\ &X_5 : (x,y) \to (\cos(\epsilon)x + \sin(\epsilon)y, -\sin(\epsilon)x + \cos(\epsilon)y); \\ &X_6 : (y,z) \to (\cos(\epsilon)y + \sin(\epsilon)z, -\sin(\epsilon)y + \cos(\epsilon)z); \\ &X_7 : (z,x) \to (\cos(\epsilon)z + \sin(\epsilon)x, -\sin(\epsilon)z + \cos(\epsilon)x). \end{aligned} \tag{5}$$

Their commutators are given by:

$$\begin{aligned} &[X_2,X_5] = -X_3, \quad [X_2,X_6] = -X_4, \quad [X_3,X_5] = X_2, \quad [X_3,X_7] = -X_4, \\ &[X_4,X_6] = X_2, \quad [X_4,X_7] = X_3, \quad [X_5,X_6] = -X_7, \quad [X_5,X_7] = -X_6, \\ &[X_6,X_7] = X_5. \end{aligned}$$

Case 2. Applying the transformation $u^* = u + v$, system (2) reduces to a semi-coupled system with the autonomous Fisher equation for u^*, being this a particular case from Table 4, number 7 in [36]. Then, for $g = g_1 v + g_2 v\ln v$ with arbitrary values of the constants g_1, g_2 and $d_1 = d_2$, $\rho_1 = \rho_2$, system (2) (see determining equations in Appendix A.2) admits the generators X_1, X_2, X_3, X_4, X_5, X_6, X_7, and the following:

$$X_8 = -ve^{-g_2 t}\partial_u + ve^{-g_2 t}\partial_v. \tag{6a}$$

This symmetry generates the following transformation group:

$$X_8 : (u,v) \to \left(-ve^{-g_2 t}\epsilon + u, ve^{-g_2 t}\epsilon\right) \tag{7}$$

Their commutator is given by $[X_1, X_8] = -X_8$.

Case 3. For $g = g_1 v + g_2$ with arbitrary values of the constants g_1, g_2 and $d_1 = d_2$, $\rho_1 = \rho_2$, system (2) (see determining equations in Appendix A.3) admits the generators X_1, X_2, X_3, X_4, X_5, X_6, X_7, and besides:

$$X_9 = -e^{-g_1 t}(u+v)\partial_u + e^{-g_1 t}(u+v)\partial_v, \tag{8a}$$

$$X_{10} = -e^{(\rho_2-g_1)t}(u+v-1)\partial_u + e^{(\rho_2-g_1)t}(u+v-1)\partial_v, \tag{8b}$$

$$X_{11} = \left(\frac{g_1^2}{g_2\rho_2}v - \frac{g_1}{g_2}v - u - v + \frac{g_1}{\rho_2}\right)\left(\partial_u - \partial_v\right). \tag{8c}$$

These symmetries generate the respective transformation groups:

$$\begin{aligned} X_9 : (u,v) \to\ & \left(-(u+v)e^{-g_1 t}\epsilon + u, (u+v)e^{-g_1 t}\epsilon + v\right); \\ X_{10} : (u,v) \to\ & \left(-(u+v-1)e^{(\rho_2-g_1)t}\epsilon + u, (u+v-1)e^{(\rho_2-g_1)t}\epsilon + v\right); \\ X_{11} : (u,v) \to\ & \left(\frac{1}{\tilde g}\left(\tilde g v - u - v + \frac{g_1}{\rho_2}\right)\left(-e^{-\tilde g\epsilon}+1\right) + u,\right. \\ & \left.\frac{1}{\tilde g}\left(\tilde g v - u - v + \frac{g_1}{\rho_2}\right)e^{-\tilde g\epsilon} + u + v - \frac{g_1}{\rho_2}\right), \end{aligned} \tag{9}$$

where $\tilde g = \dfrac{g_1^2}{g_2\rho_2} - \dfrac{g_1}{g_2}$. Their commutators are given by:

$$\begin{aligned} &[X_1,X_9] = -g_1 X_9, \quad [X_1,X_{10}] = (\rho_2 - g_1)X_{10}, \\ &[X_9,X_{11}] = -\tilde g X_9, \quad [X_{10},X_{11}] = -\tilde g X_{10}. \end{aligned}$$

4. Some symmetry reductions and exact solutions

This section is focused on exact analytical solutions that present several relevant applications in the field of mathematical biology. Lie method allows us to obtain different solutions regarding the classification from Section 3. However, due to the interest in the phenotypic switch in normoxic and hypoxic cells [11], we focus on the simulation of such scenarios. In our case, we consider a linear and quadratic phenotypic switch and a limited decrease of hypoxic cells to track the interpretability of the parameters used.

Therefore, we include a first Section 4.1 with the obtention of one solution of system (2) with biological interest, describing the dynamics between hypoxic and normoxic with several simulations in this matter. In a second Section 4.2, we present other highly nontrivial and spherically symmetric solutions generalized for the 3-D space. To obtain such solutions, we do not use the common procedure for reduction of multidimensional PDEs to ODEs. Instead, we will construct several ansätze (such as the line solitons in [39]) that allow us to reduce the original PDE system to an ODE system or to a PDE system with two independent variables. Our aim is not to obtain a general reduction, but

to construct solutions behaving in an adequate form for the biological tumor growth model. The obtention of the reduction of the PDEs in question to ODEs can be derived by applying the relevant optimal systems of three-dimensional subalgebras. In the case of the algebras $\langle X_1, X_2, X_3, X_4\rangle$ and $\langle X_5, X_6, X_7\rangle$ the relevant optimal systems can be found in Ref. [40].

4.1. An study of a solution of system (1) with biological interest

We focus on Case 1 from Section 3 with $g(V) = g_0 V$, where g_0 is the linear influence on the switch from hypoxic to normoxic cells. System (2) without restrictions on the diffusion (d_i) and proliferation (ρ_i) parameters is only invariant under translations and rotations. Therefore, we set the plane wave ansatz:

$$\xi = \lambda x + \mu y + \nu z + t, \quad u = U(\xi), \quad v = V(\xi). \tag{10}$$

The substitution of these variables into system (2) yields:

$$\begin{cases} -d_1\left(\lambda^2+\mu^2+\nu^2\right)U_{\xi\xi} + U_\xi - \rho_1(1-U-V)\,U - g(V) = 0, \\ -d_2\left(\lambda^2+\mu^2+\nu^2\right)V_{\xi\xi} + V_\xi - \rho_2(1-U-V)\,V + g(V) = 0. \end{cases} \tag{11}$$

Considering the special form of $g(V) = g_0 V(\xi)$ and with

$$\alpha^2 = \lambda^2 + \mu^2 + \nu^2 \tag{12}$$

coming from (10), we can obtain $U = U(\xi)$ from (11) in terms of $V = V(\xi)$ such as

$$U(\xi) = -\frac{d_2\alpha^2 V_{\xi\xi} + \rho_2 V^2 + g_0 V - \rho V + V_\xi}{\rho_2 V}. \tag{13}$$

We look then for solutions of the form

$$V(\xi) = C + v_0 e^{-v_1\xi}, \tag{14}$$

so that the decay of hypoxic cells into the normoxic cells is exponential, and they begin with an initial condition C. The choice of an exponential behavior is due to the fact that real cancers can indeed be unbounded, yet life constraints limit their growth in a finite time [41].

By substituting (14) into (11), this yields

$$U(\xi) = \frac{A + Be^{-v_1\xi} - \rho_2 {v_0}^2 e^{-2v_1\xi}}{\rho_2\left(C + v_0 e^{-v_1\xi}\right)},$$

where

$$A = -C^2\rho_2 - Cg_0 + C\rho_2, \tag{15a}$$

$$B = d_2 k^2 v_0 {v_1}^2 - 2C\rho_2 v_0 - g_0 v_0 + v_0\rho_2 + v_0 v_1. \tag{15b}$$

Substituting both (13) and (14) into (11), the conditions that must be verified for the system to hold can be computed. Considering that the parameters are non-zero, the following equations must be verified:

$$d_1 = \frac{C\rho_1^2 - 2C\rho_1\rho_2 + C\rho_2^2 - \rho_1^2 + \rho_2\rho_1 - \rho_1 v_1}{\alpha^2\rho_1 v_1^2}, \tag{16a}$$

$$d_2 = -\frac{1}{k^2 v_1}, \tag{16b}$$

$$g_0 = \rho_2 - \rho_2 C + \frac{\rho_2^2 C}{\rho_1}. \tag{16c}$$

A solution of the previous system is included by setting the parameters found in the literature and described in Table 1. Using such values and substituting into system (16), we were able to obtain the parameters v_1, C and g_0.

To sum up, a solution of system (2) is considered, which was obtained as

$$\begin{aligned} u = U(\xi) &= \frac{A + Be^{-v_1\xi} - \rho_2 {v_0}^2 e^{-2v_1\xi}}{\rho_2\left(C + v_0 e^{-v_1\xi}\right)}, \\ v = V(\xi) &= C + v_0 \cdot e^{-v_1\xi}, \end{aligned} \tag{17}$$

where $\xi = \xi(x, y, z, t) = \lambda x + \mu y + \nu z + t$, both (15) and (16) hold, and the function g in system (2) is given by $g(V) = g_0 V(\xi)$ with $\alpha^2 = \lambda^2 + \mu^2 + \nu^2$.

For system (2) to hold, parameters d_1 and d_2 are considered as given [11]. This leads to the computation of v_1 and C, respectively from (16a) and (16b). In the following simulations, the initial condition C is set to be close to 1, which regulates v_1 in (16a). In this model there is no affection of the tumor growth or its reduction. However, the location of the more hypoxic area is determined by the parameters λ, μ, and ν. Once parameter v_1 is set, parameter k is estimated by adjusting the three latter to be close to the original estimation of d_2 in (16b). The final parameters selected to simulate and interpret the solution (17) are those presented in Table 1. The code for estimating the parameters and generating such simulations can be found in https://github.com/salvadorchulian/hypoxia.lie.symmetries.

Considering the above, we simulated solutions in a sphere, setting the space of variables x, y, z, thus approximating the space to the shape of a tumor. Our aim would be to understand how normoxic u and hypoxic v cells are distributed in the tumor. The solutions of such a scenario are presented in Figs. 2 and 3, where cell density varies depending on the cell type.

In Fig. 2, the influence of each one of the space and time variables on the distribution of normoxic (red) and hypoxic cells (blue) can be observed. Dashed and dotted lines represent the impact of the corresponding parameter of distance influence, i.e., λ for variable x, μ for y, and ν for z. In such cases, the parameter is doubled (dashed lines) or divided by two (dotted lines). It is observed how they all have an exponential decrease for the hypoxic cells (blue) and growth for normoxic ones (red). The qualitative behavior is similar in all cases. For the case of time, the time unit was converted from hours to days for clarity of the results. The time variable is also doubled (dashed line) and divided by two (dotted line), obtaining a similar outcome.

In Fig. 3(A), it can be observed how, in the same tumor, normoxic (panel A.1) and hypoxic cells (panel A.2) distribute themselves separately. The existence of a blood vessel could be considered around the point $(1, 1, 1)$, where the normoxic cells are denser than hypoxic ones. This was set by choice of the parameters λ, μ, and ν. On the contrary, the point $(-1, -1, -1)$ could represent an area lacking oxygen.

In Fig. 3(B), slices of the center of the tumor are represented along time; this is when $z = 0$. In panel B.1, normoxic cells u tend to expand along the tumor space, even considering the hypoxic area. On the other hand, in panel B.2, hypoxic cells tend to disappear due to the appearance of normoxic cells. This can be due to the fact that hypoxic cells change their type with the function $g(v)$ to a normoxic one.

4.2. Other solutions derived from the admitted symmetries

In this subsection, a highly nontrivial solution, derived in [30], is generalized on the 3D space for system (2). Firstly, we find exact solutions of the form:

$$\xi = \lambda x + \mu y + \nu z, \quad u = U(\xi, t), \quad v = V(\xi, t). \tag{18}$$

The substitution of these variables into system (2) yields:

$$\begin{cases} -d_1\left(\lambda^2+\mu^2+\nu^2\right)U_{\xi\xi} + U_\xi - \rho_1(1-U-V)\,U - g(V) + U_t = 0, \\ -d_2\left(\lambda^2+\mu^2+\nu^2\right)V_{\xi\xi} + V_\xi - \rho_2(1-U-V)\,V + g(V) + V_t = 0. \end{cases} \tag{19}$$

Following [30], a quadratic form of function g is considered, with

$$g(V) = b_1 V^2 + b_2 V + b_3. \tag{20}$$

and we set the ansatz

$$V(\xi, t) = C_1 + k_2 \cosh\left(k_1\xi\right) e^{kt}. \tag{21}$$

For Eqs. (19) to hold, we need, with $\alpha^2 = \nu^2 + \lambda^2 + \mu^2$ that

$$b_1 = \frac{\rho_2^2}{\rho_1 - \rho_2}, \tag{22a}$$

Table 1
Parameters used for simulation in Figs. 2 and 3.

Parameter	Meaning	Value	Unit	Source
d_1	Diffusion rate of u cells	10^{-12}	cells/cm^3/s	[11]
d_2	Diffusion rate of v cells	10^{-11}	cells/cm^3/s	[11]
ρ_1	Proliferation rate of u cells	1/24	cells/h	[11]
ρ_2	Proliferation rate of v cells	1/48	cells/h	[11]
α	General parameter of influence in u level	$\approx 5.1 \cdot 10^4$	s/cm	(12)
λ	Influence of distance x in u level	$3 \cdot 10^4$	s/cm	Estimated
μ	Influence of distance y in u level	$3 \cdot 10^4$	s/cm	Estimated
ν	Influence of distance z in u level	$3 \cdot 10^4$	s/cm	Estimated
C	Initial density of hypoxic cells	≈1	cells/cm^3	(16a)
v_0	Transformation rate of u into v cells	−3/4	cells/cm^3	Estimated
v_1	Exponential decay from u into v cells	≈-0.01	1/s	(16b)
g_0	Linear influence of function $g(V)$	≈0.01	Unitless	(16c)

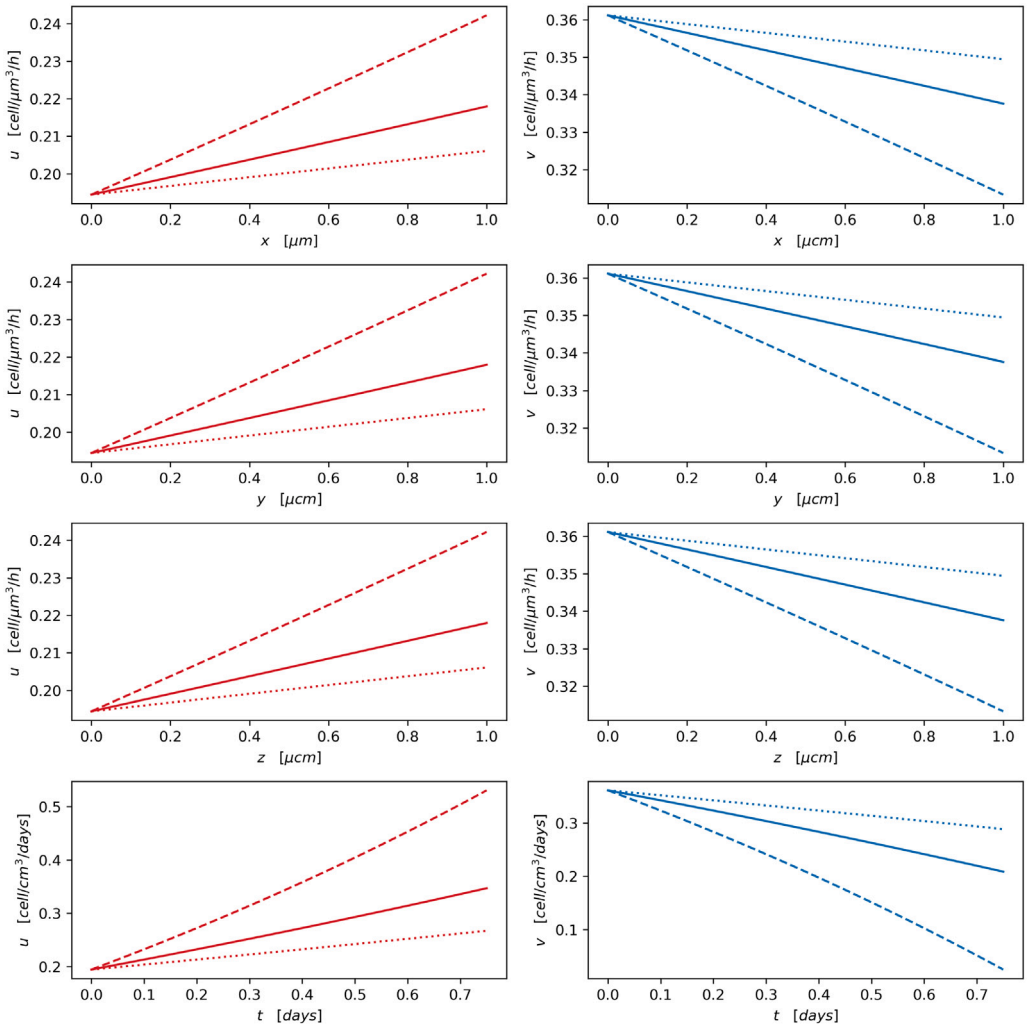

Fig. 2. Influence of each independent variable in the normoxic u and hypoxic v levels. In each row, the impact of each independent variable x, y, z, t is included, while the behavior for normoxic u and hypoxic v cells is presented in the left and right panels. Respectively, dashed and dotted lines represent multiplying or dividing by two either the distance influence parameters λ, μ, ν for x, y, z and the doubling or dividing by two the time t in the last case. Parameters used for simulation are those in Table 1.

$$b_2 = \frac{\left(1 - C_1\right)\rho_1^3 + \rho_2\left(3C_1 - 1\right)\rho_1^2 - 3\left(C_1\rho_2 - \frac{k_1(d_1-d_2)\alpha^2}{3}\right)\rho_2\rho_1 + \rho_2^3 C_1}{\rho_1\left(\rho_1 - \rho_2\right)}, \tag{22b}$$

$$b_3 = \frac{\left(\rho_2^2 C_1 + \left(\left(-2C_1 + 1\right)\rho_1 - k_1^2\left(d_1 - d_2\right)\alpha^2\right)\rho_2 + \rho_1^2\left(C_1 - 1\right)\right)C_1}{\rho_1 - \rho_2}, \tag{22c}$$

$$k = \frac{\alpha^2\rho_1 d_2 k_1^2 - \alpha^2\rho_2 d_1 k_1^2 + C_1\rho_1^2 - 2\rho_1 C_1\rho_2 + \rho_2^2 C_1 - \rho_1^2 + \rho_1\rho_2}{\rho_1 - \rho_2}, \tag{22d}$$

where C_1, k_1 and k_2 are arbitrary constants.

For this case, we verify that

$$U(\xi, t) = 1 - C_1 - \frac{\cosh\left(k_1\xi\right)\rho_2 k_2 e^{kt}}{\rho_1} \tag{23}$$

holds Eqs. (19). In Fig. 4, a representation of solutions (21) and (23) are shown.

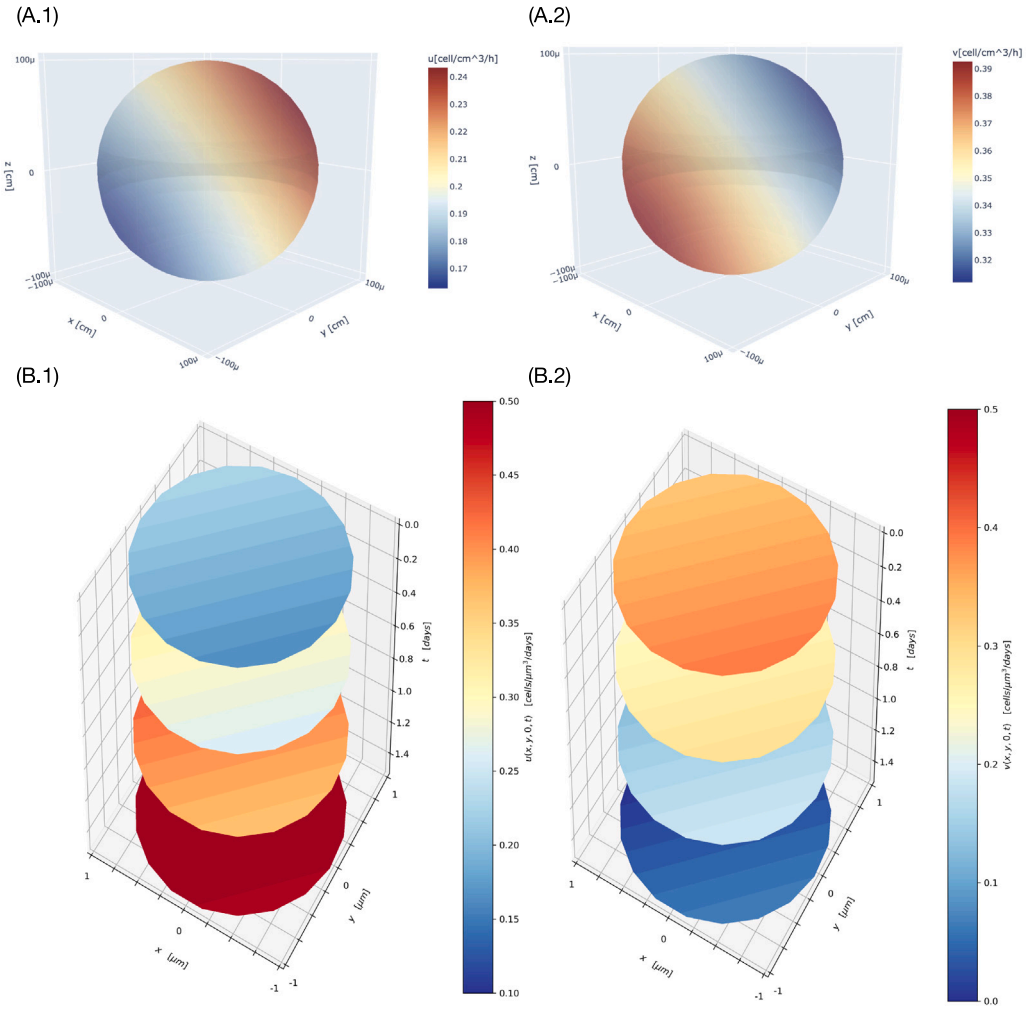

Fig. 3. 3-dimensional representation of normoxic and hypoxic levels in a tumor. (A) In panels (A.1) and (A.2), 3-dimensional representations of a sphere with the distribution of respectively normoxic and hypoxic cells in a tumor are shown. **(B)** In panels (B.1) and (B.2) slices of the $z = 0$ level of the spherical distribution are presented for normoxic and hypoxic cells in (A), as well as how they change along time t. Parameters used for simulation are those in Table 1.

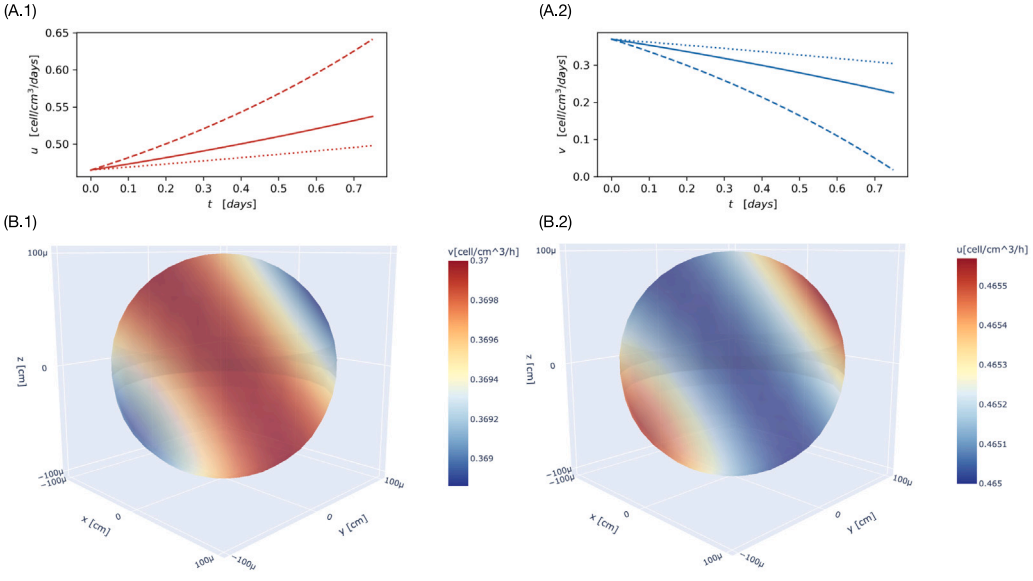

Fig. 4. Representation of solutions U and V as in (21) and (23). Panels (A.1) and (A.2) represent, respectively, the change in time for normoxic (u) and hypoxic cells (v). Panels (B.1) and (B.2), represent respectively, as well, the spatial distribution of this solution, considering the tumor to be spherically shaped. The parameters used for this representation are the followings: $\lambda, \mu, \nu = 3 \cdot 10^4$, $\rho_1 = 1/24$, $\rho_2 = 1/48$, $d_1 = 10^{-12}, d_2 = 10^{-11}$, $k_1 = 0.016$, $k_2 = -0.33$, $C = 7/10$. Parameters b_1, b_2, b_3 and k are obtained from the priors using (22).

Secondly, spherically-symmetric solutions, which are generated by the rotating Lie symmetries X_5, X_6, X_7, are derived. We consider:

$$\xi = x^2 + y^2 + z^2, \quad u = U(\xi, t), \quad v = V(\xi, t), \tag{24}$$

obtaining the reduced system

$$\begin{aligned} &-4d_1\xi U_{\xi\xi} - 6d_1 U_\xi + \rho_1 (V-1) U + \rho_1 U^2 - g(V) + U_t = 0, \\ &-4d_2\xi V_{\xi\xi} - 6d_2 V_\xi + \rho_2 (U-1) V + \rho_2 V^2 + g(V) + V_t = 0. \end{aligned} \tag{25}$$

Considering $g(V)$ with a quadratic form (see Eq. (20)), and

$$V(\xi, t) = \frac{k_1 e^{kt}}{\sqrt{\xi}}, \tag{26}$$

with k_1 an arbitrary parameter, the following system must hold

$$b_1 = \frac{-\rho_2 (\rho_1 - \rho_2)}{\rho_1}, \tag{27a}$$

$$b_2 = \rho_1, \tag{27b}$$

$$b_3 = 0, \tag{27c}$$

$$k = -\rho_1, \tag{27d}$$

yielding the solution

$$\begin{aligned} U(\xi, t) &= 1 - \frac{k_1 \rho_2}{\rho_1 \sqrt{\xi}} e^{-\rho_1 t}, \\ V(\xi, t) &= \frac{k_1 e^{-\rho_1 t}}{\sqrt{\xi}}. \end{aligned} \tag{28}$$

5. Conclusions and future work

Mathematical models in biology are a growing field, especially those that can be applied to biomedical problems. In this study, a generalized coupled system of PDEs has been examined. This system modeled biological invasions between phenotypically different cells and was analyzed from the point of view of Lie symmetries. The study of nonlinear phenomena has been a continuous source of new problems. It has motivated the introduction of new methods in mathematical analysis, partial differential equations, and other disciplines, thereby becoming one of the most active areas of mathematical research over the last decades. The investigation of exact solutions of nonlinear PDEs plays an essential role in analyzing nonlinear phenomena, particularly in obtaining analytical solutions for biomedical problems such as cancer. In this sense, the Lie symmetry method greatly simplifies many nonlinear problems.

Even if challenging to investigate, exact solutions are yielded using Lie symmetry group theory. In this paper, by using the symmetries derived in [36,37] we have provided a particular case of system (2) of biological interest, such as tumor progression due to phenotypic switching. As such, we find analytical solutions for this model and simulate the dynamics of cells depending on the oxygen levels; this is for normoxic and hypoxic cell distributions. Furthermore, we have considered the particular form of g and V based purely on the linearity of phenotypic change and the limitation of tumor growth. For the corresponding equations of the coupled system (2), we have obtained analytical solutions for a tumor progression model.

We have qualitatively studied a case that simulates the cell density behavior in a 3-dimensional space. This study is consistent with the biological description of the go or grow model exposed in Section 2, with cells having distinctive proliferative and migratory behaviors. The results in Figs. 2–4 show that both normoxic and hypoxic cells increase and decrease exponentially, respectively. The locations of the areas with higher cell density in each case were determined by the parameters obtained by the Lie symmetry analysis, i.e., λ, μ, and ν.

In future work, these features could be fitted to experimental data by, for example, considering an irregular shape of the tumor or multiple areas with different oxygenation levels. Mathematically, an extended model could improve the generalization already made here by including how the phenotypic switch can be made from normoxic to hypoxic cells. These results can be used as predictive tools to understand tumor growth dynamics.

CRediT authorship contribution statement

M. Rosa: Conceptualization, Methodology, Investigation, Writing – original draft, Formal analysis, Writing – review & editing, Validation. **M.L. Gandarias:** Methodology, Investigation, Writing – review & editing, Formal analysis, Supervision. **A. Niño-López:** Writing – review & editing, Software, Visualization. **S. Chulián:** Conceptualization, Writing – original draft, Writing – review & editing, Software, Visualization, Validation.

Declaration of competing interest

The authors declare that they have no known competing financial interests or personal relationships that could have appeared to influence the work reported in this paper.

Data availability

No data was used for the research described in the article.

Acknowledgments

The support of Junta de Andalucía Group FQM-201 is gratefully acknowledged. This work does not have any conflicts of interest.

Appendix. Determining equations for each case presented

For each of the Cases presented in the manuscript, we show the corresponding determining equations.

A.1. Determining equations for Case 1

$$\begin{cases} \tau_t = 0, \tau_x = 0, \tau_y = 0, \tau_z = 0, \\ \xi^1_t = 0, \xi^1_x = 0, \\ \xi^2_t = 0, \xi^2_y = 0, \\ \xi^3_t = 0, \xi^3_z = 0, \\ \eta^1 = 0, \eta^2 = 0, \\ \xi^2_{xx} = 0, \xi^3_{xx} = 0, \\ \xi^3_{xy} = 0, \xi^3_{yy} = 0, \\ \xi^1_y = -\xi^2_x, \\ \xi^1_z = -\xi^3_x, \\ \xi^2_z = -\xi^3_y \end{cases} \tag{A.1}$$

A.2. Determining equations for Case 2

$$\begin{cases} d_1 = d_2, \rho_1 = \rho_2, \\ \tau_t = 0, \tau_x = 0, \tau_y = 0, \tau_z = 0, \\ \xi^1_t = 0, \xi^1_x = 0, \\ \xi^2_t = 0, \xi^2_y = 0, \\ \xi^3_t = 0, \xi^3_z = 0, \\ \xi^2_{xx} = 0, \xi^3_{xx} = 0, \\ \xi^3_{xy} = 0, \xi^3_{yy} = 0, \\ \eta^2_x = 0, \eta^2_y = 0, \eta^2_z = 0, \eta^2_u = 0, \\ \xi^1_y = -\xi^2_x, \xi^1_z = -\xi^3_x, \xi^2_z = -\xi^3_y, \\ \eta^1 = -\eta^2, \eta^2_v = \frac{\eta^2}{v}, \\ g_{vv} = -\frac{g - g_v v}{v^2}, \\ \eta^2_t = \frac{-\eta^2 g_v v + \eta^2 g}{v} \end{cases} \tag{A.2}$$

A.3. Determining equations for Case 3

$$\begin{cases} d_1 = d_2, \rho_1 = \rho_2, \\ \tau_t = 0, \tau_x = 0, \tau_y = 0, \tau_z = 0, \\ \xi^1_t = 0, \xi^1_x = 0, \\ \xi^2_t = 0, \xi^2_y = 0, \\ \xi^3_t = 0, \xi^3_z = 0, \\ \xi^2_{xx} = 0, \xi^3_{xx} = 0, \\ \xi^3_{xy} = 0, \xi^3_{yy} = 0, \\ \eta^2_x = 0, \eta^2_y = 0, \eta^2_z = 0, \\ g_{vv} = 0, \\ \xi^1_y = -\xi^2_x, \xi^1_z = -\xi^3_x, \xi^2_z = -\xi^3_y, \\ \eta^2_{uu} = 0, \eta^2_{uv} = 0, \eta^2_{vv} = 0, \\ \eta^1 = -\eta^2, \\ \eta^2_t = \rho_2 \left(\eta^2_u \left(u^2 + uv\right) + \eta^2_v \left(vu + v^2\right) - u \left(\eta^2_u + \eta^2\right) - v \left(\eta^2 + \eta^2_v\right)\right) + \\ \quad +g \left(\eta^2_v - \eta^2_u\right) + \eta^2 \left(\rho_2 - g_v\right) \end{cases} \tag{A.3}$$

References

[1] Stupp R, Mason WP, Van Den Bent MJ, Weller M, Fisher B, Taphoorn MJ, et al. Radiotherapy plus concomitant and adjuvant temozolomide for glioblastoma. N Engl J Med 2005;352(10):987–96.

[2] Mangiola A, Anile C, Pompucci A, Capone G, Rigante L, De Bonis P. Glioblastoma therapy: going beyond Hercules Columns. In: Expert review of neurotherapeutics. 2010, p. 507–14.

[3] Giese A, Bjerkvig R, Berens M, Westphal M. Cost of migration: invasion of malignant gliomas and implications for treatment. J Clin Oncol 2003;21:1624–36.

[4] Pérez-García VM, Fitzpatrick S, Pérez-Romasanta LM, Pesic M, Schucht P, Arana E, et al. Applied mathematics and nonlinear sciences in the war on cancer. Appl Math Nonlinear Sci 2016;1:423–36.

[5] Hatzikirou H, Basanta D, Simon M, Schaller K, Deutsch A. 'Go or grow': the key to the emergence of invasion in tumour progression? Math Med Biol 2012;29:49–65.

[6] Martínez-González A, Calvo GF, Pérez Romasanta LA, Pérez-García VM. Hypoxic cell waves around necrotic cores in glioblastoma: a biomathematical model and its therapeutic implications. Bull Math Biol 2012;74:2875–96.

[7] Pham K, Chauviere A, Hatzikirou H, Li X, Byrne HM, Cristini V, et al. Density-dependent quiescence in glioma invasion: instability in a simple reaction–diffusion model for the migration/proliferation dichotomy. J Biol Dyn 2012;6:54–71.

[8] Alfonso J, Talkenberger K, Seifert M, Klink B, Hawkins-Daarud A, Swanson K, et al. The biology and mathematical modelling of glioma invasion: a review. J R Soc Interface 2017;14:20170490.

[9] Rosa M, Chulián S, Gandarias ML, Traciná R. Application of Lie point symmetries to the resolution of an interface problem in a generalized Fisher equation. Physica D 2020;405:132411.

[10] Chulián S, Rosa M, Gandarias ML. Symmetries and solutions for a Fisher equation with a proliferation term involving tumor development. Math Methods Appl Sci 2020;43(4):2076–84.

[11] Pardo R, Martínez-González A, Pérez-García VM. Nonlinear ghost waves accelerate the progression of high-grade brain tumors. Commun Nonlinear Sci Numer Simul 2016;39:360–80.

[12] Martínez-González A, Calvo GF, Pérez-Romansanta LA, Pérez-García VM. Hypoxic cell waves around necrotic cores in glioblastoma: A biomathematical model and its therapeutic implications. Bull Math Biol 2012;74(12):2875–96.

[13] Martínez-González A, Durán-Prado M, Calvo GF, Alcaín FJ, Pérez-Romansanta LA, Pérez-García VM. Combined therapies of antithrombotics and antioxidants delay in silico brain tumor progression. Math Med Biol 2015;32:239–62.

[14] Antal T, Krapivsky PL. Exact solution of a two-type branching process: model of tumor progression. J Stat Mech Theory Exp 2011;P08018.

[15] Greenspan HP. On the growth and stability of cell cultures and solid tumors. J Theor Biol 1976;56:229–42.

[16] Mogorosi TE, Freire IL, Muatjetjeja B, Khalique CM. Group analysis of a hyperbolic Lane–Emden system. Appl Math Comput 2017;292:156–64.

[17] Adem AR, Moretlo TS, Muatjetjeja B. A generalized dispersive water waves system: Conservation laws; symmetry reduction; travelling wave solutions; symbolic computation. In: Partial differential equations in applied mathematics. 2022, 100465.

[18] Chao-Zhong W. From additional symmetries to linearization of Virasoro symmetries. Physica D 2013;249:25–37.

[19] Olver PJ. Applications of Lie groups to differential equations, vol. 107. Berlin: Springer Science & Business Media; 1993.

[20] Bluman GW, Kumei S. Symmetries and differential equations. In: Applied mathematical sciences. Berlin: Springer; 1989.

[21] Shagolshem S, Bira B, Sil S. Conservation laws and some new exact solutions for traffic flow model via symmetry analysis. Chaos Solitons Fractals 2022;165:112779.

[22] Iskenderoglu G, Kaya D. Chirped self-similar pulses and envelope solutions for a nonlinear Schrödinger's in optical fibers using Lie group method. Chaos Solitons Fractals 2022;162:112453.

[23] Bhatti MM, Jun S, Khalique CM, Shahid A, Fasheng L, Mohamed MS. Lie group analysis and robust computational approach to examine mass transport process using Jeffrey fluid model. Appl Math Comput 2022;421:126936.

[24] Tanwar DV. Lie symmetry reductions and generalized exact solutions of Date–Jimbo–Kashiwara–Miwa equation. Chaos Solitons Fractals 2022;162:112414.

[25] Gönül S, Özemir C. Lie symmetries and traveling wave solutions of the 3D Benney–Roskes/Zakharov–Rubenchik system. Chaos Solitons Fractals 2022;165:112807.

[26] Rodrigo M, Masayasu M. Exact solutions of a competition-diffusion system. Hiroshima Math J 2000;30(2):257–70.

[27] Hung LC. Exact traveling wave solutions for diffusive Lotka–Volterra systems of two competing species. Jpn J Ind Appl Math 2012;29:237–51.

[28] Cherniha R, Dutka V. A diffusive Lotka–Volterra system: Lie symmetries, exact and numerical solutions. Ukrainian Math J 2004;56:1665–75.

[29] Cherniha R, Davydovych V. Construction and application of exact solutions of the diffusive Lotka–Volterra system: A review and new results. Commun Nonlinear Sci Numer Simul 2022;113:106579.

[30] Pliukhin O. Q-conditional symmetries and exact solutions of nonlinear reaction–diffusion systems. Symmetry 2015;7(4):1841–55.

[31] Gorin F, Harley W, Schnier J, Lyeth B, Jue T. Perinecrotic glioma proliferation and metabolic profile within an intracerebral tumor xenograft. Acta Neuropathol 2004;107:235–44. http://dx.doi.org/10.1007/s00401-003-0803-1.

[32] Murray JD. Mathematical biology. New York, Berlin, Heidelberg: Springer-Verlag; 2002.

[33] Lotka AJ. Elements of physical biology. Baltimore: Williams and Wilkins; 1925.

[34] Volterra V. Variazioni e fluttuazioni del numero d'individui in specie animali conviventi. Memoria Reale Accad Naz Lincei 1926;2:31–113.

[35] Hastings A. Global stability in Lotka–Volterra systems with diffusion. J Math Biol 1978;6:163–8.

[36] Cherniha R, King JR. Lie symmetries of nonlinear multidimensional reaction–diffusion systems: I. J Phys A Math Gen 2000;33:267–82.

[37] Cherniha R, King JR. Lie symmetries of nonlinear multidimensional reaction–diffusion systems: II. J Phys A Math Gen 2003;36:405–25.

[38] Ibragimov NH, Ibragimov NK. Elementary Lie group analysis and ordinary differential equations. New York: Wiley; 1999.

[39] Anco SC, Gandarias ML, Recio E. Conservation laws, symmetries, and line soliton solutions of generalized KP and Boussinesq equations with p-power nonlinearities in two dimensions. Theoret Math Phys 2018;197:1393–411.

[40] Patera J, Winternitz P. Subalgebras of real three-and four-dimensional Lie algebras. J Math Phys 1977;18:1449–55.

[41] Pérez-García VM, Calvo GF, Bosque JJ, León-Triana O, Jiménez J, Pérez-Beteta J, et al. Universal scaling laws rule explosive growth in human cancers. Nat Phys 2020;16(12):1232–7.